Check for updates



ADVANCED FUNCTIONAL MATERIALS
www.afm-journal.de

# Unusually Strong Near-Infrared Photoluminescence of Highly Transparent Bulk InSe Flakes

*Jamie Geng, Dehui Zhang, Inha Kim, Hyong Min Kim, Naoki Higashitarumizu, I K M Reaz Rahman, Lam Lam, Joel W. Ager III, Albert V. Davydov, Sergiy Krylyuk, and Ali Javey**

**Bulk $\gamma$-InSe has a direct bandgap of 1.24 eV, which corresponds to near infrared wavelengths ($\lambda = 1.0$ µm) useful in optoelectronic applications from biometric detectors to silicon photonics. However, its potential for optoelectronic applications is largely untapped due in part to the lack of quantitative studies of its optical properties. Here, the unusually low absorptance and high photoluminescence quantum efficiency of single-crystalline InSe flakes with thickness in the hundreds of nanometers are studied. InSe emits brightly at room temperature from its direct bandgap with a peak photoluminescence quantum yield (PLQY) of 20%, despite displaying indirect bandgap like low absorption coefficient due to the symmetry of its crystal structure. By performing pump-dependent PLQY measurements, the radiative and nonradiative recombination coefficients are extracted, including the Shockley-Read-Hall and Auger coefficients. Finally, a proof-of-concept alternating current electroluminescent device at low temperature is demonstrated to show the promise of InSe in optoelectronic technology such as highly transparent, bright NIR light sources.**

## 1. Introduction

Indium selenide ($\gamma$-InSe), a layered III-VI semiconductor, has attracted considerable interest as a material platform for electronics due to its promising electrical characteristics.[1–3] Its high electron mobility and relative stability have enabled high-performance transistors of nanometer scale.[4–8] However, its optical properties, especially in bulk, are less studied. InSe has a direct bulk bandgap of 1.24 eV, increasing to 2.1 eV as the thickness decreases to monolayer.[5,9] The rhombohedral crystal lattice of InSe is shown in **Figure 1**a. Its structure is comprised of covalently bonded layers of Se-In-In-Se, which are weakly held together by van der Waals forces in the ABC stacking order.

Unusually, InSe exhibits poor absorption of in-plane polarized light while efficiently converting out-of-plane polarized light into bright photoluminescent emission (Figure 1b).[10] InSe has a direct bandgap at all except few-layer thicknesses,[11–13] therefore boasting the efficient emission mechanism of direct bandgap materials, while absorbing light weakly like an indirect bandgap material. The combination of the high mobility, effective light emission, and low absorption coefficient in InSe may allow for the creation of fast, efficient near-infrared (NIR) photodetectors and light-emitting diodes (LEDs) that are highly transparent.

Here, we perform a quantitative study of the optical characteristics of intrinsic $\gamma$-InSe. The absorptance of InSe is remarkably weak even as its thickness increases to hundreds of nanometers. Despite low absorptance, InSe emits strongly, with peak photoluminescence quantum yield (PLQY) reaching 20% at room temperature. To elucidate the effect of different recombination processes, we perform pump-dependent photoluminescence (PL) measurements and fit them to the ABC model, from which we extract the coefficients for surface,

J. Geng, D. Zhang, I. Kim, H. M. Kim, N. Higashitarumizu, I. K. M. R. Rahman, A. Javey
Department of Electrical Engineering and Computer Sciences
University of California
Berkeley, CA 94720, USA
E-mail: ajavey@berkeley.edu

J. Geng, D. Zhang, I. Kim, N. Higashitarumizu, I. K. M. R. Rahman, J. W. Ager III, A. Javey
Materials Sciences Division
Lawrence Berkeley National Laboratory
Berkeley, CA 94720, USA

The ORCID identification number(s) for the author(s) of this article can be found under https://doi.org/10.1002/adfm.202413672

**DOI: 10.1002/adfm.202413672**

N. Higashitarumizu
JST, PRESTO
4-1-8 Honcho, Kawaguchi, Saitama 332-0012, Japan

L. Lam
Department of Chemistry
University of California Berkeley
Berkeley, CA 94720, USA

J. W. Ager III
Department of Materials Science and Engineering
University of California Berkeley
Berkeley, CA 94720, USA

A. V. Davydov, S. Krylyuk
Materials Science and Engineering Division
National Institute of Standards and Technology
Gaithersburg, MD 20899, USA



© 2024 Wiley-VCH GmbH

16163028, 2025, 3, Downloaded from https://advanced.onlinelibrary.wiley.com/doi/10.1002/adfm.202413672 by Univ of California Lawrence Berkeley National Lab, Wiley Online Library on [23/01/2025]. See the Terms and Conditions (https://onlinelibrary.wiley.com/terms-and-conditions) on Wiley Online Library for rules of use; OA articles are governed by the applicable Creative Commons License

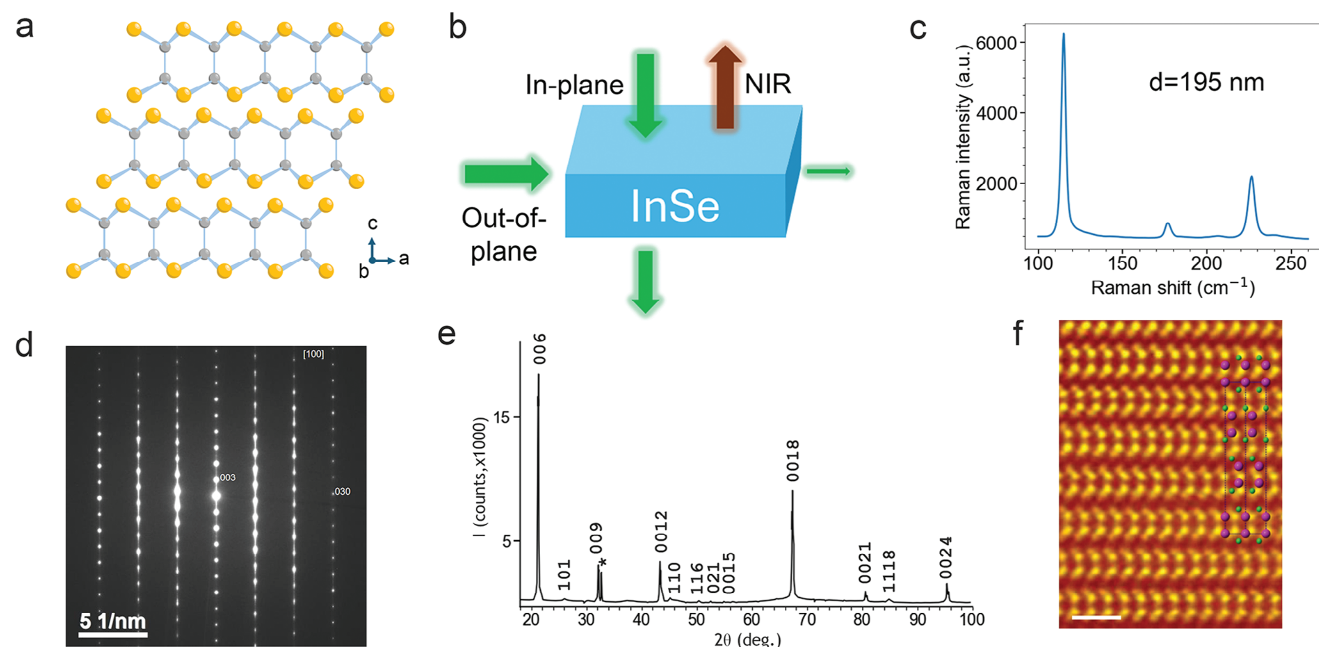


**Figure 1.** Material properties of $\gamma$-InSe. a) Crystal structure. b) Polarized absorption and emission diagram. c) Raman spectrum of a bulk InSe flake. d) Electron diffraction pattern of single-crystalline InSe. Reproduced with permission.[14] Copyright 2022, Springer Nature. e) Powder X-ray diffraction spectrum of InSe. Reproduced with permission.[12] Copyright 2024, American Chemical Society. f) Atomic-resolution scanning transmission electron microscope image of layers of atoms in exfoliated InSe crystal, with atomic model of $\gamma$-InSe structure overlayed. Reproduced with permission.[12] Copyright 2024, American Chemical Society.

Shockley-Read-Hall (SRH), Auger, and radiative recombination. We show that bandgap changes with temperature, and that at low temperature, the negligible change of PLQY with increasing pump power implies the suppression of SRH recombination. Finally, we fabricate alternating current electroluminescence (ACEL) devices and operate them at 4 K to demonstrate the feasibility of electrically pumped InSe-based NIR-emitting devices.

## 2. Results and Discussion

### 2.1. Photoluminescence Characterization

High-quality InSe was grown using the vertical Bridgman method (see, Experimental Section). Structural characterization of InSe used in this study was recently reported, with some figures reproduced in Figure 1.[12,14] We measured Raman spectra of thick flakes, which exhibited peaks at 115, 178, and 227 cm$^{-1}$, which is consistent with those of $\gamma$-InSe in prior studies.[15,16] To perform optical characterizations, InSe was mechanically exfoliated onto quartz substrates to produce a variety of flakes, whose thicknesses were measured by atomic force microscopy (AFM) (Figure S1, Supporting Information). Micro-PL spectra were measured and normalized for a range of flake thicknesses from 10 nm to several hundred nanometers to show the shift in bandgap with thickness (**Figure** 2a). The PL spectrum of thick flakes has a high-energy tail caused by a secondary contribution. InSe is known to oxidize slowly in air, with a few surface layers becoming $In_2O_3$ and causing PL degradation over a long period. However, it remains stable for hours to days.[17,18] Indeed, PL of flakes exposed to air for 90 min showed no significant difference when compared to the PL of flakes in a nitrogen chamber (Figure S2, Supporting Information). Therefore, the native oxide formed on a short timescale does not seem to affect the optical properties of bulk InSe. Flakes in this work were typically measured before 90 min of air exposure had elapsed.

Bulk flakes in the hundred-nanometer thickness range exhibit PL peaks at 1.24 eV. As flake thickness decreases, bandgap increases, rising to 1.32 eV for 10 nm flakes. Additionally, the PL intensity diminishes as flake thickness falls below 100 nm. Other studies have attributed a sharp decrease in PL intensity as InSe flakes decrease below 7 layers in thickness to a transition from direct to indirect bandgap.[11–13] However, as layers have a periodicity of 0.8 nm,[19] even the thinnest 10 nm flakes measured in this study are over 12 layers thick and above the indirect limit. Instead, surface recombination is the dominant mechanism that causes decreased PL for bulk flakes thinner than 100 nm.[20]

### 2.2. Quantitative Weak Absorptance and Strong NIR Emission

Micro-reflectance and micro-transmittance measurements were performed in ambient conditions for flakes exfoliated on quartz, with a range of flake thicknesses. A source laser with a wavelength of 532 nm and spot size of 1 μm$^2$ was focused on the top surface of each flake. Transmittance was measured by placing a photodetector below the sample and its transparent substrate, and reflectance was measured by moving the photodetector into the optical path above the flake. The absorptance is given by

$$Abs = 1 - R - T \tag{1}$$

 © 2024 Wiley-VCH GmbH

16163028, 2025, 3, Downloaded from https://advanced.onlinelibrary.wiley.com/doi/10.1002/adfm.202413672 by Univ of California Lawrence Berkeley National Lab, Wiley Online Library on [23/01/2025]. See the Terms and Conditions (https://onlinelibrary.wiley.com/terms-and-conditions) on Wiley Online Library for rules of use; OA articles are governed by the applicable Creative Commons License

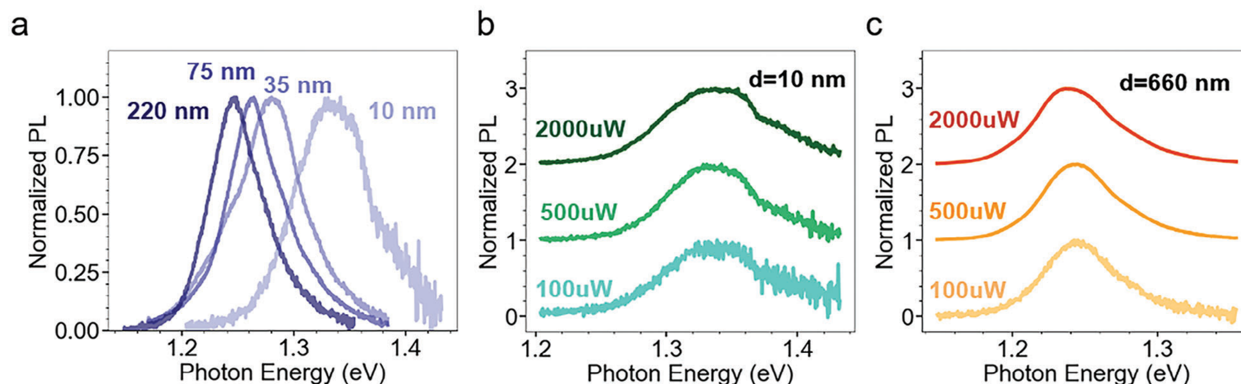


**Figure 2.** Emission spectra of $\gamma$-InSe. a) Normalized PL spectra across different thicknesses. b) PL spectra of thick bulk flake and thin 10 nm flake, showing difference in intensity.

where *Abs* is absorptance, *R* is reflectance, and *T* is transmittance. The absorptance shows a linear trend, expectedly increasing with thickness as more layers absorb more light according to the Beer-Lambert law (**Figure** 3b). However, the increase is slow, as even flakes hundreds of nanometers in thickness exhibit low absorptivity, primarily due to high transmittance. The absorption coefficient was extracted from the slope to be $5 \times 10^3$ cm$^{-1}$ at 532 nm. This aligns with values reported in prior literature, which range from $1 \times 10^3$ to $5 \times 10^4$ cm$^{-1}$.[21–24] Compared to the absorption coefficient of other direct bandgap semiconductors, the absorption coefficient of InSe is one to two orders of magnitude smaller. The weak absorption originates from selection rules determined by the crystal symmetry of InSe. The z → -z symmetry of monolayer InSe allows only transitions between states with the same symmetry across the z axis (even to even or odd to odd) for in-plane polarized light,[25] such as the perpendicular laser beam of a PL system. However, the edge states of the conduction band and valence band are respectively odd and even, resulting in the bandgap transition being prohibited for in-plane polarized light. As more layers are added, the z→ -z symmetry is weakened, and the selection rules against in-plane light bandgap transitions soften but persist.[5,10,26] Therefore, even thick flakes absorb a fraction of incident in-plane light and display high transmittance, appearing optically transparent (Figure 3a). The emitted light is also out of plane, causing measurements of PL on wrinkled flakes to be enhanced as the emission is at an angle from the vertical.[9,27]

Pump-dependent PL measurements were conducted by taking the emission spectrum of a variety of InSe flakes at a series of increasing pump powers measured by a power meter at the sideport. The pump power was subsequently converted to generation rate. PLQY was derived by integrating the measured spectrum and comparing it to the calculated generation rate. The results were plotted in **Figure** 4a. Although InSe is often considered to be an excitonic material, especially at low temperature and nanoscale thickness,[21] extrapolating measured and calculated exciton binding energies to hundred-nanometer thicknesses results in bulk binding energies that are below the thermal energy, indicating free-carrier behavior dominance in bulk.[13,28] Additionally, the pump-dependent PLQY curves for the thicknesses measured at room temperature display the rise, peak, and droop expected of free-carrier recombination dominant systems. Therefore, the resulting data was fitted to the ABC model for free carrier recombination, a simplified model for capturing recombination physics. This model considers Shockley-Read-Hall (SRH),[29,30] surface,[31,32] bimolecular radiative,[33] and Auger recombination processes (Figure 3b).[34,35] Generation rate is calculated as

$$G = \left(A + \frac{2S}{d}\right) \frac{n^2 - n_i^2}{n} + B\left(n^2 - n_i^2\right) + 2Cn\left(n^2 - n_i^2\right) \tag{2}$$

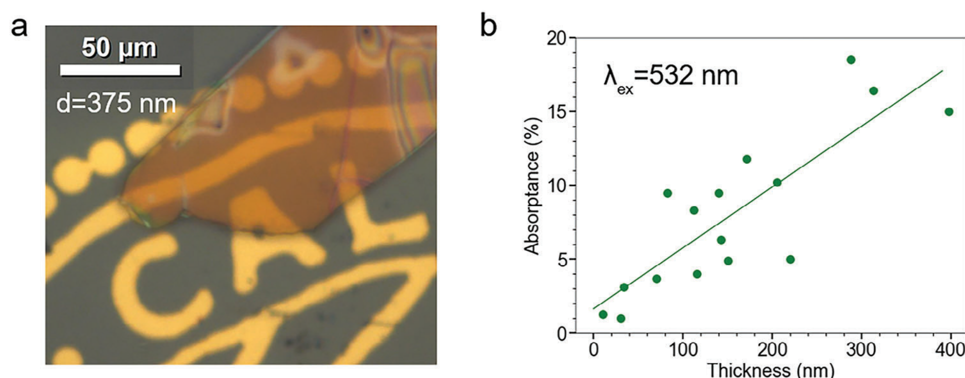


**Figure 3.** Absorptance of InSe. a) Optical microscope image showing the transparency of a thick flake. b) Absorptance trend of 532 nm laser across different thicknesses.


© 2024 Wiley-VCH GmbH

16163028, 2025, 3, Downloaded from https://advanced.onlinelibrary.wiley.com/doi/10.1002/adfm.202413672 by Univ of California Lawrence Berkeley National Lab, Wiley Online Library on [23/01/2025]. See the Terms and Conditions (https://onlinelibrary.wiley.com/terms-and-conditions) on Wiley Online Library for rules of use; OA articles are governed by the applicable Creative Commons License

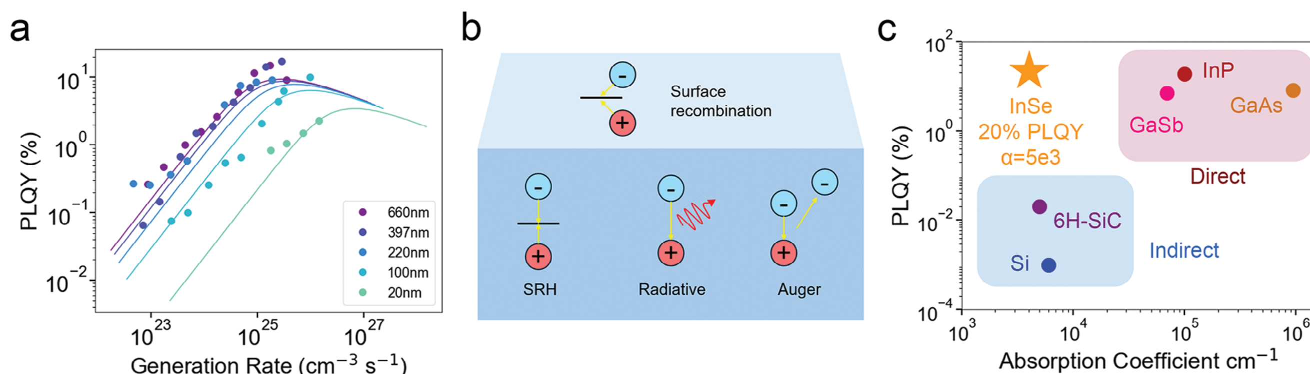


**Figure 4.** PLQY and recombination. a) PLQY of flakes of different thicknesses across increasing pump power, fitted with the ABC model for carrier recombination. b) Schematic of different recombination processes modeled. c) Comparison of absorption coefficients and peak PLQY of various semiconductors.

where $G$ is generation rate, $n$ is carrier concentration, $n_i$ is intrinsic carrier concentration, and $A$, $B$, $C$, and $S$ are respectively SRH, radiative, Auger, and surface recombination coefficients. These recombination pathways are summarized in Figure 4b. PLQY is calculated as

$$QY = \frac{B\left(n^2 - n_i^2\right)}{G} \tag{3}$$

The measured data aligns closely with this model (Figure 4a), which assumes that the dominant recombination pathway is highly dependent on the number of carriers required for each process, and the generation rate. At low generation rates, PLQY increases with generation rate, indicating the dominance of single-carrier trap-assisted SRH recombination.[36] Additionally, in the low generation regime, the PLQY is sensitive to thickness. Flakes above 100 nm in thickness exhibit similar PLQY curves, but thinner flakes show decreased PLQY. Flakes of 20 nm are nearly an order of magnitude less efficient than bulk flakes. This points to the presence of surface recombination, another form of trap-assisted recombination, which begins to affect the PLQY characteristics more strongly as the thickness decreases, and surface area becomes more dominant. The PLQY peaks at intermediate generation rates, where radiative recombination is dominant. As generation rate continues to increase, PLQY is lowered by the rising dominance of three-carrier, nonradiative Auger recombination.[37] The data was quantitatively fit by first calculating B to be $4.2 \times 10^{-9}$ cm$^3$ s$^{-1}$ from

$$B = \frac{1}{\tau_r n_i} \tag{4}$$

using previously reported values of 8 ns for radiative lifetime ($\tau_r$) and $3 \times 10^{16}$ cm$^{-3}$ for as-grown carrier concentration ($n_i$).[38,39] Then, A, C, and S were determined by fitting to be $4 \times 10^8$ cm$^{-1}$, $4 \times 10^{-25}$ cm$^6$ s$^{-1}$, and $4 \times 10^3$ s$^{-1}$ respectively. The SRV coefficient S is an order of magnitude lower than that determined by previous work,[23] while quantitative values for the other coefficients has not been established for InSe. A, B, and C consistent with other common semiconductor systems.

InSe has high PL efficiency for an unpassivated, unencapsulated semiconductor, peaking at 20% PLQY for thick flakes above 100 nm. This quantum efficiency is enabled by several factors. First, as a 2D van der Waals material, InSe lacks surface dangling bonds that enhance nonradiative recombination pathways.[40,41] The high quality of the grown InSe source also results in a low density of defects that can lower PLQY. Finally, InSe maintains a direct bandgap at bulk thicknesses unlike other commonly studied 2D materials such as transition metal dichalcogenides (TMDs),[42,43] allowing efficient radiative recombination at higher thicknesses not dominated by surface traps as shown by the increase of PLQY with thickness in Figure 4a.

A 20% PLQY is not unprecedented- perfectly passivated silicon and high-quality indium phosphide also exhibit near or above 20% efficiency.[44,45] Figure 4c plots the PLQY and absorption constant of a range of unpassivated, chemically untreated semiconductor materials. The direct bandgap III-V semiconductors InP, GaAs, and GaSb present middling or good PLQY in conjunction with higher absorptivity, and are therefore used frequently for solar cells and NIR or visible photodetectors and LEDs. In the low absorptivity, low quantum efficiency quadrant is unpassivated silicon and 6H-SiC, which are poor absorbers and emitters due to indirect bandgaps, and more challenging to use in optoelectronic applications. Among common semiconductors with well-documented quantum yields, InSe alone exhibits both high PLQY and low absorptivity. In other words, it appears to absorb like indirect bandgap silicon and emit like a direct bandgap III-V semiconductor. Notably, InSe does not require perfect passivation or any other treatment to achieve high quantum yields.

### 2.3. Low Temperature Photoluminescence and Quantum Yield Measurements

To study the effects of temperature on PLQY and bandgap, thick samples were cooled down to low temperatures and measured with variable pump power, with results shown in **Figure 5**. At 4 K, the PLQY of the sample remains constant across low generation rates, indicating suppression of nonradiative pathways. The value of the PLQY is over 60%, triple the peak value at room temperature. Low temperature is known to suppress SRH


© 2024 Wiley-VCH GmbH

16163028, 2025, 3, Downloaded from https://advanced.onlinelibrary.wiley.com/doi/10.1002/adfm.202413672 by Univ of California Lawrence Berkeley National Lab, Wiley Online Library on [23/01/2025]. See the Terms and Conditions (https://onlinelibrary.wiley.com/terms-and-conditions) on Wiley Online Library for rules of use; OA articles are governed by the applicable Creative Commons License

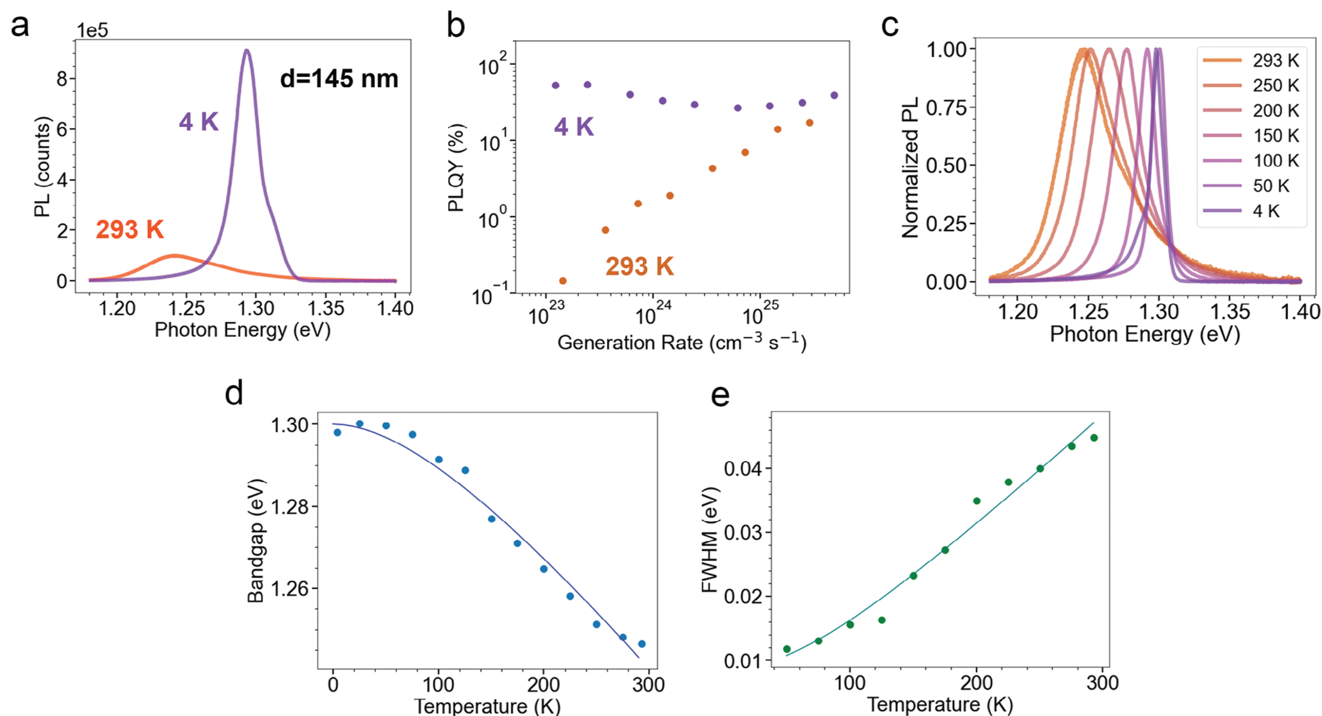


**Figure 5.** Temperature dependence of photoluminescence of InSe flakes. a) Comparison of room temperature and low temperature spectra and photon counts. b) Power-dependent PLQY of flake at room temperature and 4 K. c) Temperature dependent spectra of a single flake. d) Change in bandgap with temperature, fit with the Varshni equation. e) Temperature dependent full width at half maximum, fit with a phonon model.

recombination because carriers lack the thermal energy to jump to trap states where they may recombine non-radiatively.[30,46] The finding that PLQY is strongly enhanced at low generation rates supports our analysis that recombination is dominated by SRH. Additionally, as the sample cools, the spectral peak blueshifts from 1.24 to 1.30 eV. This indicates the shrinking of lattice dimensions and decreasing of phonon-electron interactions with decreasing temperature causing an increased bandgap.[21] This data was fit to the Varshni equation (Figure 5d)

$$E_g\ (T) = E_g\ (0) + \frac{\alpha T^2}{T + \beta} \tag{5}$$

where the bandgap at 0 K $E_g$ was found to be 1.30 eV, and the Varshni parameters $\alpha$ and $\beta$ were found to be $3.46 \times 10^{-4}$ eV K$^{-1}$ and 222 K respectively.[47]

Spectral peaks also widen significantly with increasing temperature, from a full width at half maximum (FWHM) of 9.1 meV at 4 K to a FWHM of 44 meV at 293 K in Figure 5c. This is due to the increase of the broadening parameter with temperature, as phonon-electron interactions increase and shorten the carrier lifetime.[21] To further analyze phonon interactions, the temperature-dependent FWHM was fit with the following model

$$\mathrm{FWHM}\ (T) = \Gamma_0 + \Gamma_a T + \Gamma_{\mathrm{op}} \frac{1}{\exp\left(\frac{\hbar\omega_{LO}}{k_B T}\right) - 1} \tag{6}$$

where $\Gamma_0$ represents the temperature-independent inhomogeneous broadening, $\Gamma_a$ is the acoustic phonon coupling coefficient, $\Gamma_{op}$ is the optical phonon coupling coefficient, and $\omega_{LO}$ is the energy of the longitudinal optical (LO) phonon (Figure 5e). Based on prior work, the LO phonon frequency was set to 199 cm$^{-1}$.[48] The fitting resulted in a $\Gamma_0$ of 6.9 meV, an $\Gamma_a$ of 0.075 meV K$^{-1}$ and a $\Gamma_{\mathrm{op}}$ of 30 meV. The low $\Gamma_0$ suggests that the material is high quality with few defects or impurities that could contribute to temperature-independent broadening of linewidth. Additionally, the low $\Gamma_a$ compared to $\Gamma_{op}$ indicates that acoustic phonons contribute only moderately to FWHM increase with temperature, while optical phonons dominate the linewidth broadening with increasing temperature.

### 2.4. Demonstration of Alternating Current Electroluminescence Device

To demonstrate that InSe may be used for electroluminescence (EL), we fabricated a simple alternating-current electroluminescence (ACEL) device,[49,50] consisting of a gold contact evaporated over an InSe flake, on 50 nm $SiO_2$/Si substrate. The device structure is shown in **Figure 6a**. This structure comprises a metal-oxide-semiconductor (MOS) capacitor, where InSe is the semiconductor, the $SiO_2$ layer is the oxide, and the highly doped Si substrate is the metal gate. The evaporated gold layer serves as the top contact. Although only one gold contact is used per ACEL device, two are shown fabricated in Figure 6a to allow for two devices per flake, as

ACEL is tightly localized to the interface between material and contact.[50] Only one contact on the flake is biased during operation, while the other is left floating. Initial photolithography runs

 © 2024 Wiley-VCH GmbH

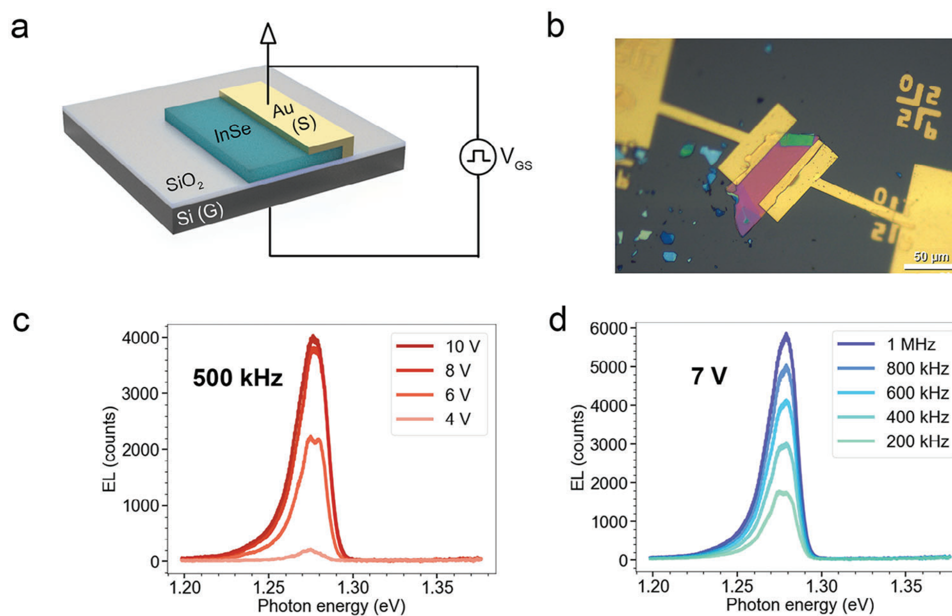


**Figure 6.** InSe light-emitting capacitor. a) Schematic showing device structure. b) Optical image of fabricated device. c) Voltage dependent electroluminescence (EL) spectra at 4 K. d) Frequency-dependent EL spectra at 4 K.

using a bilayer photoresist combination of LOR and Microposit S1818 revealed that thick InSe flakes are prone to delaminating from the $Si/SiO_2$ substrate when the LOR underlayer was applied via spin-coating. Without LOR, liftoff in PG remover for evaporated layers of 5 nm Ti / 200 nm was unclean, leading to device shorting. Additionally, PG remover also caused some delamination of the InSe flakes. To avoid these issues, a strategy of e-beam lithography with PMMA resist, evaporating no Ti and 200 nm gold for the contacts, and liftoff in gentler acetone was developed.

Briefly, to produce EL, the device is driven with an alternating voltage $V_{GS}$, applied to one gold contact and the silicon back gate. At positive $V_{GS}$, electrons accumulate in the semiconductor, while few holes are present. When $V_{GS}$ initially switches to negative, a large electric field is applied across the semiconductor-Au contact interface, causing significant band bending in the semiconductor. A high concentration of holes can then tunnel into the semiconductor before the electrons can flow out through the contact. These carriers recombine in the semiconductor near the interface, emitting light. This proof-of-concept device bypasses the need for the transport layers and very fine bandgap engineering for efficient injection of holes and electrons required for direct current devices.

At room temperature, no EL was measured upon electrical excitation with a square wave at several different peak voltages and frequencies, indicating that charge injection is too low at reasonable voltages to reach the generation regime in which emission is efficient. To achieve detectable emission at low generation rate, the device was cooled to 4 K. The measured EL intensity increases with increasing peak $V_{GS}$ due to more extreme band bending and thinning of the tunneling barrier, plateauing ≈8 V when driven at 500 kHz (Figure 6c). Increasing frequency also enhances measured EL by raising the number of transient EL pulses in a collection period (Figure 6d).

ACEL devices have been demonstrated with other materials at room temperature. In contrast to our bulk InSe devices, previous studies used ultra-thin emissive layers such as monolayer TMDs, 12 nm Si layers, and single layers of organic dyes.[51–53] The thinness of these emissive materials allows for a high concentration of injected charge through the contacts, while the thick InSe in our devices results in a far lower charge density. To achieve detectible luminescence, the InSe devices were cooled to 4 K to leverage the enhanced luminescence due to suppression of nonradiative SRH recombination and dominance of excitonic effects at cryogenic temperatures. While these findings show that ACEL devices are not the optimal structures for creating effective bulk InSe emitters, the success of these simple low-temperature devices suggests that with further device optimization, InSe could serve as an efficient electroluminescent emitter.

## 3. Conclusion

Layered 2D materials are promising for a variety of applications, from high-performance 2D transistors that challenge the silicon scaling limit, to flexible sensors. With its strong emission in the NIR, InSe stands out as an optoelectronic material because it is both remarkably transparent and an efficient emitter. This work focuses on in-plane measurements, so future work on optical characteristics may include a deeper quantitative study of the anisotropic PL of InSe, especially including excitation with out-of-plane photons. Our work with low temperature measurements and fabrication of basic devices demonstrates the potential of InSe for further efficiency enhancement, and for technological applications. InSe may not be the best candidate for applications requiring efficient absorption, but it shows promise as an electrically pumped emitter for transparent LEDs due to its high PLQY. Device structures and bandgap engineering must be investigated and the challenge of 2D scalability addressed for InSe to

 © 2024 Wiley-VCH GmbH

16163028, 2025, 3, Downloaded from https://advanced.onlinelibrary.wiley.com/doi/10.1002/adfm.202413672 by Univ of California Lawrence Berkeley National Lab, Wiley Online Library on [23/01/2025]. See the Terms and Conditions (https://onlinelibrary.wiley.com/terms-and-conditions) on Wiley Online Library for rules of use; OA articles are governed by the applicable Creative Commons License

realize its full potential as a low-cost, efficient emitter with atypical characteristics.

## 4. Experimental Section

*Crystal Growth*: Intrinsic InSe single-crystalline ingots (1 cm diameter, 3 cm length) were grown by the vertical Bridgman method using pre-synthesized polycrystalline In1.04Se0.96 charge that was loaded in a graphitized quartz ampoule and sealed under vacuum. The melt was equilibrated for 3 h at 720 °C and then the ampoule was translated across a temperature gradient at a rate of 0.5 mm $h^{-1}$.

*Device Fabrication*: EL devices were fabricated by first mechanically exfoliating InSe onto 50 nm $SiO_2$/Si substrates. 150–300 nm thick, large flakes were identified by microscope and marked, then confirmed by AFM step profile. 200 nm thick gold contacts were formed on each selected flake by electron lithography and evaporation. Liftoff of excess gold was performed in acetone. The completed devices were mounted to a Montana cryostation mount with silver paste, and wire-bonded to electrical connections.

*Optical Characterization*: PL measurements were carried out with a homebuilt micro-PL system with a 532 nm line source under ambient conditions. The 532 nm excitation beam was directed through a 50× Mitutoyo NIR objective by a series of mirrors and a periscope and focused on the sample surface with the aid of a camera. The resulting emission spectra were collected through the same objective and directed using another set of mirrors and a periscope to a NIR detector (Andor iDus InGaAs) connected to a spectrograph (Andor Shamrock 500i). The power of the source was measured with a Thorlabs power meter at a sideport before the objective. The instrument response function of the entire setup was measured by directing a Thorlabs SLS201 Lambertian light source onto a Spectralon reflector, and comparing the measured spectrum with the vendor SLS201 spectrum. The collection efficiency was determined by focusing a 940 nm LED with known intensity onto a Spectralon reflector and measuring the response. Micro-reflectance measurements were taken on the same PL system with a photodetector (Thorlabs PDA36A) in the reflectance path and lock-in detection. Micro-transmittance measurements were also performed on this setup with the photodetector moved under the sample holder. These optical setups are illustrated in the Supporting Information, in Figures S4 and S5 (Supporting Information). Low temperature PL measurements were conducted with the sample under vacuum in a Montana Cryostation s200. EL measurements were also conducted in this Cryostation using the electrical connections on the sample mount. Square waves were provided by an Agilent 33522A arbitrary wavefunction generator. All spectra measurements were corrected for the instrument response function.

*Model Fitting*: All models were fit to data in Python using Scipy curve_optimize, which utilizes least-squares optimization to find the best fit of a user defined model to the given data.

## Supporting Information

Supporting Information is available from the Wiley Online Library or from the author.

## Acknowledgements

This work was funded by the US Department of Energy, Office of Science, Office of Basic Energy Sciences, Division of Materials Sciences and Engineering under contract no. DE-AC02-05Ch11231 (Electronic Materials program). N.H. acknowledges support from JST PRESTO (JPMJPR23H7), Japan. S.K. and A.V.D. acknowledge support from the Material Genome Initiative funding allocated to NIST.

## Conflict of Interest

The authors declare no conflict of interest.

## Data Availability Statement

The data that support the findings of this study are available from the corresponding author upon reasonable request.

## Keywords

electroluminescence, indium selenide, near-infrared, photoluminescence quantum yield, weak absorption

Received: July 29, 2024
Revised: September 10, 2024
Published online: September 23, 2024

[1] G. Han, Z.-G. Chen, J. Drennan, J. Zou, *Small* **2014**, *10*, 2747.
[2] D. W. Boukhvalov, B. Gürbulak, S. Duman, L. Wang, A. Politano, L. S. Caputi, G. Chiarello, A. Cupolillo, *Nanomaterials* **2017**, *7*, 372.
[3] D. Zheng, P. Chen, Y. Liu, X. Li, K. Liu, Z. Yin, R. Frisenda, Q. Zhao, T. Wang, *J. Mater. Chem. A* **2024**, *12*, 16952.
[4] K. Imai, K. Suzuki, T. Haga, Y. Hasegawa, Y. Abe, *J. Cryst. Growth* **1981**, *54*, 501.
[5] D. A. Bandurin, A. V. Tyurnina, G. L. Yu, A. Mishchenko, V. Zólyomi, S. V. Morozov, R. K. Kumar, R. V. Gorbachev, Z. R. Kudrynskyi, S. Pezzini, Z. D. Kovalyuk, U. Zeitler, K. S. Novoselov, A. Patanè, L. Eaves, I. V. Grigorieva, V. I. Fal'ko, A. K. Geim, Y. Cao, *Nat. Nanotechnol.* **2017**, *12*, 223.
[6] J. Jiang, L. Xu, C. Qiu, L.-M. Peng, *Nature* **2023**, *616*, 470.
[7] T.-H. Tsai, F.-S. Yang, P.-H. Ho, Z.-Y. Liang, C.-H. Lien, C.-H. Ho, Y.-F. Lin, P.-W. Chiu, *ACS Appl. Mater. Interfaces* **2019**, *11*, 35969.
[8] J. Jiang, J. Li, Y. Li, J. Duan, L. Li, Y. Tian, Z. Zong, H. Zheng, X. Feng, Q. Li, H. Liu, Y. Zhang, T.-L. Ren, L. Han, *NPJ 2D Mater. Appl.* **2019**, *3*, 29.
[9] M. Brotons-Gisbert, D. Andres-Penares, J. Suh, F. Hidalgo, R. Abargues, P. J. Rodríguez-Cantó, A. Segura, A. Cros, G. Tobias, E. Canadell, P. Ordejón, J. Wu, J. P. Martínez-Pastor, J. F. Sánchez-Royo, *Nano Lett.* **2016**, *16*, 3221.
[10] C. Song, S. Huang, C. Wang, J. Luo, H. Yan, *J. Appl. Phys.* **2020**, *128*, 060901.
[11] G. W. Mudd, S. A. Svatek, T. Ren, A. Patanè, O. Makarovsky, L. Eaves, P. H. Beton, Z. D. Kovalyuk, G. V. Lashkarev, Z. R. Kudrynskyi, A. I. Dmitriev, *Adv. Mater.* **2013**, *25*, 5714.
[12] N. A. Pike, R. Pachter, M. A. Altvater, C. E. Stevens, M. Klein, J. R. Hendrickson, H. Zhang, S. Krylyuk, A. V. Davydov, N. R. Glavin, *J. Phys. Chem. C* **2024**, *128*, 7957.
[13] A. Ceferino, K. W. Song, S. J. Magorrian, V. Zólyomi, V. I. Fal'ko, *Phys. Rev. B* **2020**, *101*, 245432.
[14] J. Miao, C. Leblanc, J. Wang, Y. Gu, X. Liu, B. Song, H. Zhang, S. Krylyuk, W. Hu, A. V. Davydov, T. Back, N. Glavin, D. Jariwala, *Nat. Electron.* **2022**, *5*, 744.
[15] M. Wu, Q. Xie, Y. Wu, J. Zheng, W. Wang, L. He, X. Wu, B. Lv, *AIP Adv.* **2019**, *9*, 025013.
[16] N. Balakrishnan, E. D. Steer, E. F. Smith, Z. R. Kudrynskyi, Z. D. Kovalyuk, L. Eaves, A. Patanè, P. H. Beton, *2D Mater.* **2018**, *5*, 035026.
[17] L. Shi, Q. Zhou, Y. Zhao, Y. Ouyang, C. Ling, Q. Li, J. Wang, *J. Phys. Chem. Lett.* **2017**, *8*, 4368.
[18] Q. Xie, C. Hu, L. Xu, L. Chen, W. Wang, H. Yin, G. Cheng, X. Ai, *Solid State Commun.* **2021**, *336*, 114417.
[19] T.-R. Wei, M. Jin, Y. Wang, H. Chen, Z. Gao, K. Zhao, P. Qiu, Z. Shan, J. Jiang, R. Li, L. Chen, J. He, X. Shi, *Science* **2020**, *369*, 542.
[20] D. E. Aspnes, *Surf. Sci.* **1983**, *132*, 406.
[21] J. Camassel, P. Merle, H. Mathieu, A. Chevy, *Phys. Rev. B* **1978**, *17*, 4718.


© 2024 Wiley-VCH GmbH

16163028, 2025, 3, Downloaded from https://advanced.onlinelibrary.wiley.com/doi/10.1002/adfm.202413672 by Univ of California Lawrence Berkeley National Lab, Wiley Online Library on [23/01/2025]. See the Terms and Conditions (https://onlinelibrary.wiley.com/terms-and-conditions) on Wiley Online Library for rules of use; OA articles are governed by the applicable Creative Commons License

[22] X. Huang, Q. Cao, M. Wan, H.-Z. Song, *Materials* **2022**, *15*, 6214.
[23] C. Zhong, V. K. Sangwan, J. Kang, J. Luxa, Z. Sofer, M. C. Hersam, E. A. Weiss, *J. Phys. Chem. Lett.* **2019**, *10*, 493.
[24] R. W. Damon, R. W. Redington, *Phys. Rev.* **1954**, *96*, 1498.
[25] V. Zólyomi, N. D. Drummond, V. I. Fal'ko, *Phys. Rev. B* **2014**, *89*, 205416.
[26] S. J. Magorrian, V. Zólyomi, V. I. Fal'ko, *Phys. Rev. B* **2016**, *94*, 245431.
[27] Y. Li, T. Wang, H. Wang, Z. Li, Y. Chen, D. West, R. Sankar, R. K. Ulaganathan, F. Chou, C. Wetzel, C.-Y. Xu, S. Zhang, S.-F. Shi, *Nano Lett.* **2018**, *18*, 5078.
[28] J. Zultak, S. J. Magorrian, M. Koperski, A. Garner, M. J. Hamer, E. Tóvári, K. S. Novoselov, A. A. Zhukov, Y. Zou, N. R. Wilson, S. J. Haigh, A. V. Kretinin, V. I. Fal'ko, R. Gorbachev, *Nat. Commun.* **2020**, *11*, 125.
[29] R. N. Hall, *Semiconductor Devices: Pioneering Papers*, World Scientific, Singapore **1991**.
[30] W. Shockley, W. T. Read, *Phys. Rev.* **1952**, *87*, 835.
[31] D. J. Fitzgerald, A. S. Grove, *Surf. Sci.* **1968**, *9*, 347.
[32] K. R. McIntosh, L. E. Black, *J. Appl. Phys.* **2014**, *116*, 014503.
[33] W. P. Dumke, *Phys. Rev.* **1957**, *105*, 139.
[34] A. R. Beattie, P. T. Landsberg, *Proc. R. Soc. Lond. Ser. Math. Phys. Sci.* **1959**.
[35] A. Haug, *J. Phys. C Solid State Phys.* **1983**, *16*, 4159.
[36] G. Bemski, *Proc. IRE* **1958**, *46*, 990.
[37] V. N. Abakumov, V. I. Perel, I. N. Yassievich, *Nonradiative Recombination in Semiconductors*, Elsevier, Amsterdam, Netherlands **1991**.
[38] N. T. Paylaga, C.-T. Chou, C.-C. Lin, T. Taniguchi, K. Watanabe, R. Sankar, Y. Chan, S.-Y. Chen, W.-H. Wang, *Npj 2D Mater. Appl.* **2024**, *8*, 12.
[39] F. J. Manjón, A. Segura, V. Muñoz-Sanjosé, G. Tobías, P. Ordejón, E. Canadell, *Phys. Rev. B* **2004**, *70*, 125201.
[40] Y. Lei, T. Zhang, Y.-C. Lin, T. Granzier-Nakajima, G. Bepete, D. A. Kowalczyk, Z. Lin, D. Zhou, T. F. Schranghamer, A. Dodda, A. Sebastian, Y. Chen, Y. Liu, G. Pourtois, T. J. Kempa, B. Schuler, M. T. Edmonds, S. Y. Quek, U. Wurstbauer, S. M. Wu, N. R. Glavin, S. Das, S. P. Dash, J. M. Redwing, J. A. Robinson, M. Terrones, *ACS Nanosci. Au* **2022**, *2*, 450.
[41] M. Chhowalla, H. S. Shin, G. Eda, L.-J. Li, K. P. Loh, H. Zhang, *Nat. Chem.* **2013**, *5*, 263.
[42] K. F. Mak, C. Lee, J. Hone, J. Shan, T. F. Heinz, *Phys. Rev. Lett.* **2010**, *105*, 136805.
[43] Q. H. Wang, K. Kalantar-Zadeh, A. Kis, J. N. Coleman, M. S. Strano, *Nat. Nanotechnol.* **2012**, *7*, 699.
[44] A. W. Blakers, A. Wang, A. M. Milne, J. Zhao, M. A. Green, *Appl. Phys. Lett.* **1989**, *55*, 1363.
[45] X. Li, M. W. Wanlass, T. A. Gessert, K. A. Emery, T. J. Coutts, *Appl. Phys. Lett.* **1989**, *54*, 2674.
[46] R. Pässler, *Phys. Status Solidi B* **1978**, *85*, 203.
[47] Y. P. Varshni, *Physica* **1967**, *34*, 149.
[48] C. Song, F. Fan, N. Xuan, S. Huang, C. Wang, G. Zhang, F. Wang, Q. Xing, Y. Lei, Z. Sun, H. Wu, H. Yan, *Phys. Rev. B* **2019**, *99*, 195414.
[49] Y. Z. Wang, D. D. Gebler, L. B. Lin, J. W. Blatchford, S. W. Jessen, H. L. Wang, A. J. Epstein, *Appl. Phys. Lett.* **1996**, *68*, 894.
[50] V. Wang, Y. Zhao, A. Javey, *Adv. Mater.* **2021**, *33*, 2005635.
[51] I. K. M. R. Rahman, S. Z. Uddin, H. Kim, N. Higashitarumizu, A. Javey, *Appl. Phys. Lett.* **2022**, *121*, 193502.
[52] D.-H. Lien, M. Amani, S. B. Desai, G. H. Ahn, K. Han, J.-H. He, J. W. Ager, M. C. Wu, A. Javey, *Nat. Commun.* **2018**, *9*, 1229.
[53] J. Kim, V. Wang, S. C. Kim, J. Y. Lee, A. Javey, *Nano Lett.* **2023**, *23*, 5822.


© 2024 Wiley-VCH GmbH

16163028, 2025, 3, Downloaded from https://advanced.onlinelibrary.wiley.com/doi/10.1002/adfm.202413672 by Univ of California Lawrence Berkeley National Lab, Wiley Online Library on [23/01/2025]. See the Terms and Conditions (https://onlinelibrary.wiley.com/terms-and-conditions) on Wiley Online Library for rules of use; OA articles are governed by the applicable Creative Commons License